Focusing: coming to the point in metamaterials

S. Guenneau[a,b*], A. Diatta[b] and R.C. McPhedran[c]

August 3, 2021

[a] *Institut Fresnel, UMR CNRS 6133, University of Aix-Marseille,*
case 162, F13397 Marseille Cedex 20, France
Email: guenneau@liv.ac.uk;
[b] *Department of Mathematical Sciences, Liverpool L693BX, UK*
Email: adiatta@liv.ac.uk;
[c] *IPOS, School of Physics, University of Sydney NSW, Australia*
Email: ross@physics.usyd.edu.au

Abstract

This paper reviews some properties of lenses in curved and folded optical spaces. The point of the paper is to show some limitations of geometrical optics in the analysis of subwavelength focusing. We first provide a comprehensive derivation for the equation of geodesics in curved optical spaces, which is a tool of choice to design metamaterials in transformation optics. We then analyse the resolution of the image of a line source radiating in the Maxwell fisheye and the Veselago-Pendry slab lens. The former optical medium is deduced from the stereographic projection of a virtual sphere and displays a heterogeneous refractive index $n(r)$ which is proportional to the inverse of $1 + r^2$. The latter is described by a homogeneous, but negative, refractive index. It has been suggested that the fisheye makes a perfect lens without negative refraction [Leonhardt, Philbin arXiv:0805.4778v2]. However, we point out that the definition of super-resolution in such a heterogeneous medium should be computed with respect to the wavelength in a homogenized medium, and it is perhaps more adequate to talk about a conjugate image rather than a perfect image (the former does not necessarily contains the evanescent components of the source). We numerically find that both the Maxwell fisheye and a thick silver slab lens lead to a resolution close to $\lambda/3$ in transverse magnetic polarization (electric field pointing orthogonal to the plane). We note a shift of the image plane in the latter lens. We also observe that two sources lead to multiple secondary images in the former lens, as confirmed from light rays travelling along geodesics of the virtual sphere. We further observe resolutions ranging from $\lambda/2$ to nearly $\lambda/4$ for magnetic dipoles of varying orientations of dipole moments within the fisheye in transverse electric polarization (magnetic field pointing orthogonal to the plane). Finally, we analyse the Eaton lens for which the source and its image are either located within a unit disc of air, or within a corona $1 < r < 2$ with refractive index $n(r) = \sqrt{2/r - 1}$. In both cases, the image resolution is about $\lambda/2$.

1   Introduction

In 1967, the Russian physicist Victor Veselago wrote a visionary paper in which materials with a negative refractive index were theorized [1]. Veselago pointed out that this could happen only if the real parts of both dielectric permittivity ϵ and magnetic permeability μ are simultaneously negative at a given frequency ω. It was argued by a ray analysis that a slab of such a negative index material (NIM) can act as a flat lens that imaged a source on one side to a point on the other. But this result remained an academic curiosity for almost thirty years, until Sir John Pendry and co-workers [2, 3] proposed designs of structured materials which would have effectively negative ε and μ. However, this very unlikely event occurs only in a very narrow range of frequencies and in real life, NIM are necessarily dissipative and dispersive. Interestingly, one of us studied together with Graeme Milton and Nicolae-Alexandru Nicorovici the electrostatic response of a coated cylinder with negative ϵ back in 1994 [4], and this can be also considered as a perfect lens in the intense near field limit in transverse electric polarization [5, 6, 7].

In 2000, the experimental demonstration of a negative refractive index at GHz frequencies by a team led by David Smith [8] provided a fillip to research in this area (see [9, 10] for recent reviews). One should note that these metamaterials are structured at subwavelength lengthscales (typically one tenth of the wavelength) and it is possible to regard them as homogeneous and describe their response by dispersive effective medium parameters (see [11] for a comprehensive survey on homogenization theory). Potential applications of negative refraction came when Pendry demonstrated that the Veselago slab lens not only involves the propagation waves but also the evanescent near-field components of a source in the image formation[12]. However, there is still some limitation to the resolution (which is hardly surprising given the laws of physics), which can only become infinite in the limit of zero absorption, even though it is possible to improve the lens resolution by considering multilayered negatively refracting lenses or by adding some gain [13, 14, 15].

In 2006, the physicists John Pendry, David Schurig and David Smith theorized that a finite size object surrounded by a spherical coating consisting of a metamaterial might become invisible for electromagnetic waves [16]. This proposal has been experimentally validated the same year in the microwave regime using a two-dimensional configuration [17]. The same year, Ulf Leonhardt independently proposed a conformal map route towards cloaking [18, 19], which is valid in the geometrical optics limit (when the wavelength is much smaller than the diffracting obstacle). Both proposals actually derive from the earlier study by Allan Greenleaf, Yaroslav Kurylev, Matti Lassas, and Gunther Uhlmann [20] whereby the conductivity of an object was much reduced.

However, an alternative route towards cloaking using anomalous resonances in negatively refracting cylindrical lenses based upon the earlier work by McPhedran, Nicorovici and Milton [6] in 1994, shows that transformation optics and perfect lensing are intimately linked. A perfect lens can be seen as a multi-valued map whereby a source is mapped twice onto itself (a NIM is in essence a folded optical space) as first shown by Ulf Leonhardt and Thomas Philbin [21] and then further investigated by Milton et al. [7] and subsequently by one of us with S. Anantha Ramakrishna [22]. Using such transformation optics tools, it was also shown that two corners of NIM combined in a checkerboard fashion can act as a unique resonator [23, 24, 25, 26]. Such checkerboards and can be themselves mapped onto three dimensional corner reflectors [27] and they actually exhibit some form of extraordinary transmission [28].

Furthermore, in 2008 Ulf Leonhardt and Thomas Tyc proposed an improved type of cloaking [29], based upon a stereographic projection of a sphere onto a flat plane, leading to a non singular nearly perfect cloak. A stereographic projection is a particular mapping that projects a sphere onto a plane. The projection is defined on the entire sphere, except at one point, the projection point. Where it is defined, the mapping is smooth and bijective. It is conformal, meaning that it

preserves angles. It is neither an isometry nor area-preserving: that is, it preserves neither distances nor the areas of figures. Using such a conformal mapping, Leonhardt and Tyc further designed some super antennas [30, 31]. However, the materials resulting from these optical transformations are highly heterogeneous, and it is therefore legitimate to ask whether they fall within a class of super resolution optical systems and indeed specify in which sense they could be considered as high-resolution devices. This question is of foremost importance as some researchers have recently shown that simple enough tomography devices beat the diffraction limit [32], however with the constraint that the source be located close to a structured surface (a grating) and therefore perfect lensing occurs only in the near field limit.

The plan of the paper is as follows: following this first introductory section, we discuss in section 2 the variational framework associated with Fermat's principle, also known as principle of least time, which is the idea that the path taken between two points by a ray of light is the path that can be traversed in the least time. Section 3 is then devoted to the design of the Maxwell fisheye and the Veselago-Pendry lens through transformation optics. Section 4, the core of the paper, addresses the issue of whether the fisheye can be considered as a perfect lens without negative refraction. We look both at the cases of a fisheye of infinite extent and a fisheye surrounded by perfect conducting boundaries, as first introduced by Ulf Leonhardt in 2009 [33]. Section 5 discusses the issue of multiple (mirage) images within the fisheye when there are two or more sources. Section 6 is devoted to the analysis of the Eaton lens, which shares common some features with the mirror fisheye. Finally, section 7 draws concluding remarks.
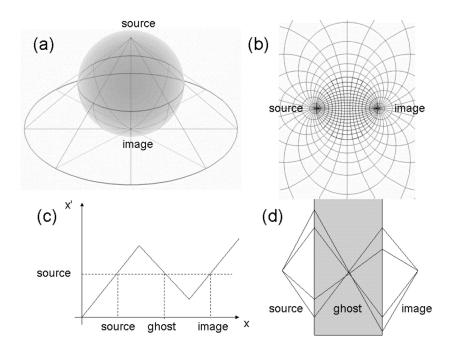

Figure 1: *Upper panel: The Maxwell fish eye; (a) Stereographic projection of a virtual sphere onto a physical plane; A source has an antipodal image on a great circle (or ray trajectory); (b) Geodesics (or ray trajectories) between a source and its image on the physical plane. Lower panel: The Veselago-Pendry slab lens (adapted from [35]); (c) Coordinate transformation from the physical x-axis to the virtual axis x'; The inverse transformation from x' to x is either triple- or single-valued. The triple-valued segment on the physical x-axis corresponds to the focal region of the lens; (d) A source point has two images on the physical axis i.e. one inside the lens (a ghost image) and one on the other side (a perfect image).*

3

2 Geometry of geodesics on a sphere

Let us consider the sphere $S^2 = \{(x', y', z') \in \mathbb{R}^3 \text{ with } x'^2 + y'^2 + z'^2 = r_0^2\}$ of radius r_0, as shown in Fig. 1(a). Ray trajectories follow so-called geodesics (great circles) on this sphere i.e. shortest trajectories. A geodesic x^i, for a metric g_{ij} is a curve $t \mapsto x^i(t)$ which is a minimum of the integral path

$$\int_a^b ds = \int_a^b \sqrt{g_{ij} \frac{dx^i(t)}{dt} \frac{dx^j(t)}{dt}} \, dt := \int_a^b \sqrt{g_{ij} \dot{x}^i \dot{x}^j} \, dt \tag{1}$$

between two points a and b in a curved space.

In transformation optics, the principle of least action of Pierre de Fermat is often invoked to deduce that the eikonal equation (linking the electric field intensity to the gradient electric potential) which describes the phase front of waves (in the ray optics limit) admits a geodesic as a local solution. Unfortunately, a global solution e.g. a solution for all time in the geometrical optics case is not possible. The reason is that caustics may develop which means that wavefronts cross. When the ray optics picture breaks down, it is then necessary to solve the vector Maxwell equations which are always valid in a linear context.

For the sake of completeness, let us establish with basic arguments that the equation of geodesics reads

$$g_{ij} \ddot{x}^j(s) + \frac{1}{2} g_{lj,i} \dot{x}^l(s) \dot{x}^j(s) = 0 \,, \tag{2}$$

where $g_{lj,i}$ denotes the derivative of g_{lj} with respect to x^i.

In classical optics, the eikonal equation is known to be valid when the wavelength λ is small in comparison to the size of the diffracting obstacle. However, in highly-heterogeneous media such as metamaterials deduced from non-Euclidean transformations, one should also take into account the effect of the optical space curvature which should be small on scales compatible with wavelengths, that is $\mid R \mid \ll \omega^2/c^2$, where R is the scalar curvature $R = g^{ij} R_{ij}$ [29]: local space curvature should not be on the same scale as the electromagnetic wave oscillations. We note that in the case of the sphere which has obviously non zero curvature, the eikonal equation is a good approximation to describe trajectories of light only when the wavelength is much smaller than the radius of the sphere.

To establish (2), let us consider the classical minimization problem:

$$\mathcal{P} : \inf_{\mathbf{x} \in C^1([a,b], S^2)} \left\{ E(\mathbf{x}) = \int_a^b L(t, \mathbf{x}(t), \dot{\mathbf{x}}(t)) \, dt \; ; \; \mathbf{x}(a) = \alpha \,, \; \mathbf{x}(b) = \beta \right\}$$

where $L = g_{ij} \dot{x}^i \dot{x}^j \in C^2([a,b] \times S^2 \times \mathbb{R}^3, \mathbb{R})$ i.e. L is a continuous function with continuous second derivatives such that $L : (t, v, \xi) \in [a,b] \times S^2 \times \mathbb{R}^3 \to L(t, v, \xi) \in \mathbb{R}$.

For α and β close enough in S^2, let $\mathbf{x} \in C^2([a,b], S^2)$ be a minimum of E in the convex set K:

$$K_{\alpha,\beta} = \{\mathbf{v} \in C^1([a,b], S^2) \,, \; \mathbf{v}(a) = \alpha \,, \; \mathbf{v}(b) = \beta\}$$

Then, we can write that for every $\phi \in C^1([a,b], \mathbb{R}^3)$ with $\phi(a) = \phi(b) = \mathbf{0}$, and for every $\theta \in]-1, 1[$ such that $\mathbf{x} + \theta\phi \in S^2$ [1]

$$E(\mathbf{x}) \leq E(\mathbf{x} + \theta\phi) \,.$$

In particular, we are assured that [2]

$$\left\{ \frac{d}{d\theta} E(\mathbf{x} + \theta\phi) \right\}_{|\theta=0} = 0 \,.$$

---

[1] Take e.g. ϕ such that $\mathbf{x}(t) + \frac{\theta}{2} \phi(t)$ is orthogonal to $\phi(t)$ and $\phi(a) = \phi(b) = \mathbf{0}$.

[2] We use the fact that $\mathbf{x} \in C^2([a,b], \mathbb{R}^3)$ since differentiating E involves differentiating the integral of $L(t, \mathbf{x}, \dot{\mathbf{x}})$ over $[a,b]$ which requires $\ddot{\mathbf{x}}$ to be continuous on $[a,b]$.

This leads us to

$$\left\{ \frac{d}{d\theta} \int_a^b L(t, \mathbf{x}(t) + \theta\phi(t), \dot{\mathbf{x}}(t) + \theta\dot{\phi}(t)) \, dt \right\}_{|\theta=0} = 0 \; .$$

Thus, we obtain

$$\int_a^b \left\{ \frac{\partial L}{\partial v} \phi + \frac{\partial L}{\partial \xi} \dot{\phi} \right\} dt = 0 \; .$$

This equation holds for any $\phi \in C^1([a, b], \mathbb{R}^3)$ such that $\phi(a) = \phi(b)$ and $\theta\phi \in S^2$, hence integrating by parts we have

$$\int_a^b \left\{ \frac{\partial L}{\partial v^i} - \frac{d}{dt} \frac{\partial L}{\partial \xi^i} \right\} \phi \, dt = 0 \; .$$

Applying the fundamental lemma of variational calculus [34], we are assured that for every $t \in (a, b)$,

$$\frac{d}{dt} \left[\frac{\partial}{\partial \xi} L(t, \mathbf{x}(t), \dot{\mathbf{x}}(t)) \right] = \frac{\partial}{\partial v} L(t, \mathbf{x}(t), \dot{\mathbf{x}}(t)) \; .$$

The geodesics are thus given as solutions of the Euler-Lagrange equations, which take the following form:

$$\frac{d}{dt} \left[g_{ij} \dot{x}^j(t) \right] = g_{lj,i} \dot{x}^l(t) \dot{x}^j(t) \; .$$

This leads us to (2)

$$g_{ij} \frac{d^2 x^i(s)}{ds^2} + g_{lj,i} \frac{dx^l(s)}{ds} \frac{dx^j(s)}{ds} = \frac{1}{2} g_{lj,i} \frac{dx^l(s)}{ds} \frac{dx^j(s)}{ds} \; ,$$

and may be further simplified [3].
Using the expression

$$ds^2 = r_0^2 (d\theta^2 + \sin^2\theta \, d\phi^2) \; , \tag{3}$$

for the metric on the surface of a sphere of radius r_0, it can be checked that geodesics on a sphere are nothing but the great circles. We note that this expression cannot be reduced to the Euclidean form $ds^2 = (dx^1)^2 + (dx^2)^2$, which shows that the surface of a sphere is not a Euclidean space (it has non-zero curvature).

3 Design of the Maxwell fisheye and the Veselago-Pendry lens through transformation optics

In this section, we use the conventional notation $\{x, y, z\} = \{x^1, x^2, x^3\}$ for the Euclidean system of coordinates. Whereas the derivation of the refractive index within the Maxwell fish eye can be found in the literature (see [35] for a comprehensive review), we include it for completeness.

Let us consider the sphere $S^2 = \{(x', y', z') \in \mathbb{R}^3 \text{ with } x'^2 + y'^2 + z'^2 = r_0^2\}$ of radius r_0, as shown in Fig. 1(a). A line element on the virtual sphere of radius r_0 is given by:

$$ds^2 = dx'^2 + dy'^2 + dz'^2 \; , \text{ with } \; x'^2 + y'^2 + z'^2 = r_0^2 \; . \tag{4}$$

Using the stereographic projection:

$$x = \frac{x'}{1 - z'/r_0} \; , \; y = \frac{y'}{1 - z'/r_0} \; ,$$

---

[3]Indeed, by multiplying this equation by the inverse tensor g^{ij} from the left and introducing the Christoffel symbol $\Gamma^i_{jk} = \frac{1}{2} g^{il}(g_{lj,k} + g_{lk,j} - g_{jk,l})$, we obtain $\ddot{x}^k(s) + \Gamma^k_{ij}(s)\dot{x}^i(s)\dot{x}^j(s) = 0$, where the Γ^k_{ij}'s are the Christoffel symbols of the Levi-Civita connection of g.

together with the inverse formula

$$x' = \frac{2x}{1 + (r/r_0)^2} \ , \ y' = \frac{2y}{1 + (r/r_0)^2} \ , \ z' = r_0 \frac{(r/r_0)^2 - 1}{1 + (r/r_0)^2} \qquad (5)$$

where $r^2 = x^2 + y^2$, and substituting in expression (4), we end up with the expression for a line element in the projected plane:

$$ds^2 = P dx^2 + Q dx dy + R dy^2 \qquad (6)$$

where

$$P = \left(\frac{\partial x'}{\partial x}\right)^2 + \left(\frac{\partial y'}{\partial x}\right)^2 + \left(\frac{\partial z'}{\partial x}\right)^2 ,$$

$$Q = \frac{\partial x'}{\partial x}\frac{\partial x'}{\partial y} + \frac{\partial y'}{\partial x}\frac{\partial y'}{\partial y} + \frac{\partial z'}{\partial x}\frac{\partial z'}{\partial y} \ , \ R = \left(\frac{\partial x'}{\partial y}\right)^2 + \left(\frac{\partial y'}{\partial y}\right)^2 + \left(\frac{\partial z'}{\partial y}\right)^2 .$$

In our particular case of the sphere and using the above expression (5) of the inverse of the stereographic projection, we get $Q = 0$ and $P = Q$, so that the corresponding line element on the projected plane simplifies into:

$$ds^2 = n^2(dx^2 + dy^2) \ , \ n = \frac{2r_0^2}{x^2 + y^2 + r_0^2} \ . \qquad (7)$$

Let us now apply these mathematical tools to the slab perfect lens which is interesting inter alia since it corresponds to a non-one-to-one coordinate transformation. This is clear, since it has triplets of planes on which the field distributions are identical: the object plane, the internal image plane and the external image plane. In the one-dimensional case, the corresponding coordinate transformation maps these three planes from a single plane in the reference space. Consider the coordinate transformation of Fig. 1(c) which is given by

$$x' = x - d \ , \text{ if } x' < d/2, \text{ or } -x \text{ if } -d/2 < x' < d/2, \text{ or } x + d \text{ if } d/2 < x' \qquad (8)$$

where d is the thickness of the lens.

This leads to the identity transformation outside the lens, whereas inside the lens i.e. for $-d/2 < x' < d/2$, the derivative of $x(x')$ becomes negative as $dx/dx' = -1$ which flips the sign of n. Moreover, there is no change in y and z coordinates, so that the material properties differ from free space only in the $x = x'$ direction, with $n = -1$ inside the lens and $n = +1$ outside. However, dx/dx' is undefined at $x' = \pm d/2$ and so is n at these interfaces.

4   A perfect lens without negative refraction?

As pointed out in the abstract, there might be an ambiguity in the definition of a perfect image in metamaterials, which are highly heterogeneous structures. We therefore decided to address this issue using full wave computations Thanks to the cylindrical geometry, the problem splits into TM and TE polarizations:

$$\nabla \times (\nabla \times \mathbf{E}_l) - \mu_0 \varepsilon_0 \omega^2 n^2 \mathbf{E}_l = -i\omega I_s \mu_0 \delta_{\mathbf{r}_s} \mathbf{e}_z \ , \qquad (9)$$

$$\nabla \times \left(n^{-2}\nabla \times \mathbf{H}_l\right) - \mu_0 \varepsilon_0 \omega^2 \mathbf{H}_l = \nabla \times (n^{-2}\mathbf{j}_T), \qquad (10)$$

where $\mathbf{E}_l = E_3(x,y)\mathbf{e}_z$, $\mathbf{H}_l = H_3(x,y)\mathbf{e}_z$ $\varepsilon_0\mu_0 = 1/c^2$, with c the celerity of light in vacuum, and ω the wave frequency. Here, the refractive index $n = n(x,y)$ is defined by (7) in the case of the Maxwell fisheye. Moreover, $\mathbf{j}_T$ in (10) denotes a current with a vanishing $z-$component.

We note that in the TE case, the right-hand side of (10) shows that the very definition of the source, for instance a magnetic dipole generated by a current circulating on a closed loop, depends upon the surrounding medium. In a heterogeneous medium, the field radiated by the source appears to be deformed by the spatially varying refractive index n. To avoid additional numerical technicalities in the finite element implementation and to simplify the physical discussion, we focus on the TM case in the sequel, except in subsection 4.3, in order to foster numerical efforts towards the complete modelling of TE polarisation.

4.1 Silver slab lens versus Maxwell's fisheye in unbounded domains

The unbounded domain is modelled using perfectly matched layers (PMLs), which are reflectionless heterogeneous anisotropic media introduced by Berenger fifteen years ago [37]. Nowadays, in the time harmonic case, the most natural way to introduce PMLs is to consider them as maps on a complex space [38, 39] so that the corresponding change of (complex) coordinates leads to equivalent ε and μ (that are complex, anisotropic, and inhomogeneous even if the original ones were real, isotropic, and homogeneous). This leads automatically to an equivalent medium with the same impedance as the one of the initial ambient medium since ε and μ are transformed in the same way and this insures that the interface with the layer is non-reflecting at all incidences.

In the present study, the cylindrical PML is an annulus whose characteristics are associated with the complex matrix [39]

$$\mathbf{T}_{PML}^{-1} = \mathbf{R}(\theta)\mathbf{diag}(\frac{\tilde{\rho}}{s_\rho \rho}, \frac{s_\rho \rho}{\tilde{\rho}}, \frac{s_\rho \tilde{\rho}}{\rho})\mathbf{R}(-\theta) \, , \tag{11}$$

with $\mathbf{R}(\theta)$ the rotation matrix by an angle θ in the xy-plane. This expression is the metric tensor in Cartesian coordinates (x, y, z) for the cylindrical PML. $\theta, \rho, \tilde{\rho}$, and $s_\rho(\rho)$ are explicit functions of the variables x and y, i.e. $\theta = 2\arctan\left(\frac{y}{x+\sqrt{x^2+y^2}}\right)$, $\rho = \sqrt{x^2+y^2}$, $s_\rho(\rho) = s_\rho(\sqrt{x^2+y^2})$, and $\tilde{\rho} = \int_0^{\sqrt{x^2+y^2}} s_\rho(\rho')d\rho'$ where $s_\rho(\rho')$ is an arbitrary but well chosen complex valued function of a real variable that describes the radial stretch relating the initial radial distance ρ to the complex one $\tilde{\rho}$.

In this annulus, the governing equation (9) takes the following form:

$$\nabla \times \left(\mathbf{T}_{PML}^{-1}\nabla \times \mathbf{E}_l\right) - \mu_0\varepsilon_0\omega^2 n^2 \mathbf{T}_{PML}^{-1}\mathbf{E}_l = \mathbf{0} \, . \tag{12}$$

We first consider the case of a refractive index with opposite signs in a lens and the surrounding medium in (9), with n set to the positive value 1 in the governing equation (12) for the annulus. To preserve the (hypo) ellipticity of the formulation, it is necessary to consider a small positive imaginary part to n in (9) for the negatively refracting medium (e.g. modelling absorption in metal for visible wavelengths). We thus consider $n = 1$ (air) in the surrounding medium and $n = -1 + i * 0.4$ (silver) in the lens. When the image is formed in the same homogeneous medium as the source such as it is the case of such a Veselago-Pendry slab lens, one shall compute the square modulus of the field in the image plane and take the full-width at half maximum of the profile to compute the resolution of the image, see Figs. 2(a) and 3(a) for the case of a silver slab lens displaying a resolution of $\lambda/3$. Interestingly, the image forms in an image plane shifted by half a wavelength (equal to half the width of the lens) compared with the theoretical prediction of the geometric transform (8). We attribute this to the imaginary part of the refractive index, which is in fact both spoiling the image resolution (through absorption) and the mirror effect about the mid-axis of the lens. We note that Pendry's poor-man lens was experimentally shown to display a resolution of $\lambda/6$ by Zhang's team back in 2005 [36]. However, the source was located in the close neighborhood of a thin film of silver i.e. in the intense near field limit. Here the image forms at a finite distance from the lens, yet not exactly according to the inverted Snell-Descartes laws of refraction. We numerically checked that when we reduce the imaginary part of the negative refractive index, the image forms closer to the predicted image plane, and the resolution increases (the full-width at half maximum of the profile narrows).

In the classical book by Born and Wolf [40], an optical system is said to produce sharp imaging of an object-point $\mathbf{x}_O$ onto an image point $\mathbf{x}_I$ when any ray trajectory emitted from $\mathbf{x}_O$ through the optical system will pass through $\mathbf{x}_I$ in an exact way. However, this definition might be misleading, as the reconstruction of the image does not necessarily involve the evanescent components of the source, thereby not beating Rayleigh's diffraction limit.

Still in Born and Wolf [40], points $\mathbf{x}_O$ and $\mathbf{x}_I$ are said to be perfect conjugates, and in our opinion this definition is more accurate for the Maxwell fisheye. For instance, the prolate ellipsoidal
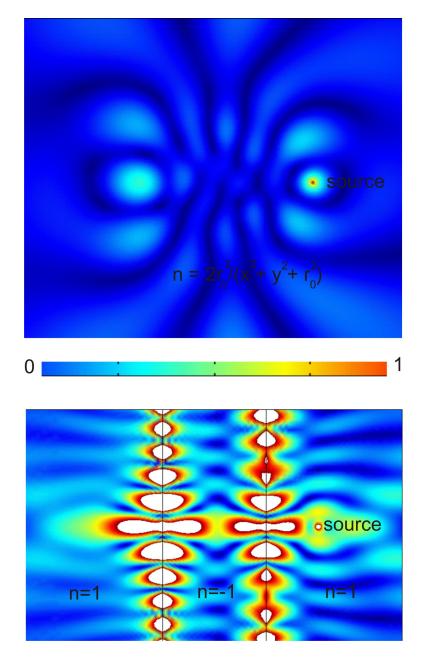
Figure 2: *2D plot of the longitudinal electric field* $| E_3 |$: *(a) Lensing effect in the Veselago-Pendry silver slab lens* $(\varepsilon = -1 + i * 0.4)$; *The harmonic line source (electric current) at free space wavelength* $\lambda_f = 0.1$ *is located a distance* 0.1 *away from the rightmost interface of the slab, and the image appears a distance* 0.1 *away from the leftmost interface; (b) Lensing effect in the Maxwell fisheye associated with a virtual sphere of radius* $r_0 = 0.1$. *The line source (electric current) at free space wavelength* $\lambda_f = 0.1$ *is located at point* $(0.1, 0)$ *and the image appears at point* $(-0.1, 0)$ *(note the astigmatism); The image appears in the non-uniform refractive index in the Maxwell fisheye whereas in the 'perfect' lens, the image is formed in vacuum but appears shifted with respect to the theoretical prediction.*

reflector is a well-known example of a perfect imaging optical system, but only for points $\mathbf{x}_O$ and $\mathbf{x}_I$ coincident with the foci of the ellipsoid, and it does not involve reconstruction of an image
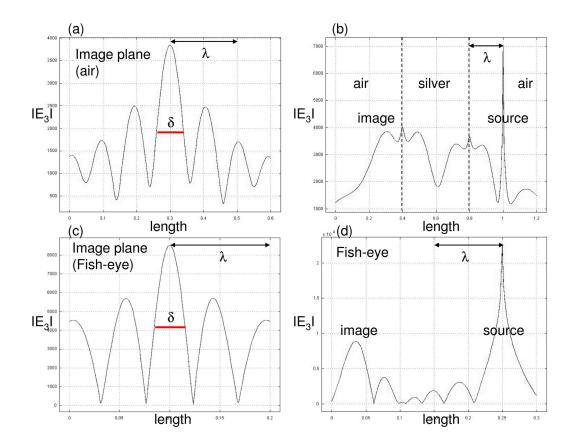
Figure 3: *Upper panel: Modulus of the longitudinal electric field E_3 radiated by a harmonic line source (electric current) at free space wavelength $\lambda_f = 0.2$, a distance 0.2 from a silver slab lens; (cf. lower panel of Fig. 2); (a) Profile along the vertical direction in the plane $x_1 = 0.3$ (whereas the theoretical prediction for the image plane is $x_1 = 0.2$). The red line represents the resolution of the image: full width at half maximum of the 'image-point' is $\delta \sim \lambda/3$, where $\lambda = \lambda_f$; (b) Profile of $\mid E_3 \mid$ in the plane $x_2 = 0$ with a source at $x_1 = 1$, a ghost image at $x_1 \sim 0.6$ and an image at $x_1 \sim 0.3$ (we note the large amplitudes at the interfaces $x_1 = 0.4$ and $x_1 = 0.6$); Lower panel: Modulus of the longitudinal electric field E_3 radiated by a harmonic line source (electric current) at free space wavelength $\lambda = 0.1$ in the Maxwell Fisheye associated with a virtual sphere of radius $r_0 = 0.1$ (cf. upper panel of Fig. 2); (c) Profile along the vertical direction in the image plane $x_1 = 0.03$ The red line represents the resolution of the image: full width at half maximum of the image-point is $\delta \sim \lambda/3$, where $\lambda < \lambda_f$ is the 'averaged wavelength' in the fisheye computed from the source to the image planes; (d) Profile of $\mid E_3 \mid$ in the plane $x_2 = 0$ with the source at $x_1 = 0.25$ and an image at $x_1 = 0.03$.*

with both propagating and evanescent components of the source (a necessary condition to beat the diffraction limit). It seems therefore fair to call such a lens a conjugate imaging optical system.

A class of conjugate imaging optical systems has been obtained in curved lenses such as the generalized Maxwell fisheyes in [41]. To construct these less than usual lenses, we consider the

following mapping from the sphere to the xy Cartesian plane

$$x = \left(\frac{1 - \sin\theta}{\cos\theta} \right)^{1/p} \cos(\frac{\phi}{p}) \ , \ y = \left(\frac{1 - \sin\theta}{\cos\theta} \right)^{1/p} \sin(\frac{\phi}{p}) \ , \tag{13}$$

where p is an integer.

Noting that the radius of the sphere S^2 is $r_0 = 1/p$, it is easily seen that

$$ds^2 = \frac{(d\theta)^2 + (\cos\theta d\phi)^2}{p^2} = n^2(dx^2 + dy^2) \ , \ n = \frac{2(x^2 + y^2)^{(p-1)/2}}{(x^2 + y^2)^p + 1} \ . \tag{14}$$

Indeed, from (13) the total derivatives of x and y can be expressed as

$$dx = \frac{1}{p} \left(\frac{1 - \sin\theta}{\cos\theta} \right)^{1/p} \left(-\frac{\cos(\frac{\phi}{p})}{\cos(\theta)} d\theta - \sin(\frac{\phi}{p})d\phi \right) \ ,$$

$$dy = \frac{1}{p} \left(\frac{1 - \sin\theta}{\cos\theta} \right)^{1/p} \left(-\frac{\sin(\frac{\phi}{p})}{\cos(\theta)} d\theta + \cos(\frac{\phi}{p})d\phi \right) \ ,$$

so that

$$dx^2 + dy^2 = \frac{1}{p^2} \left(\frac{1 - \sin\theta}{\cos\theta} \right)^{2/p} \left(\frac{1}{\cos^2(\theta)} d\theta^2 + d\phi^2 \right) \ , \tag{15}$$

and (14) follows by noting that $n = \cos(\theta) \left(\frac{\cos\theta}{1 - \sin\theta} \right)^{1/p}$.

When $p = 1$, (14) reduces to (7), for which any object point $\mathbf{x}_O$ is imaged in a point $\mathbf{x}_I$ such that $\mathbf{x}_O = -\mathbf{x}_I/\mathbf{x}_I^2$, as can be checked from Fig. 3(d).

However, at least in the TM polarisation case, we will see in the next subsection that such lenses cannot be called perfect in the sense of Pendry's perfect lens, as the image does not contain subwavelength components of the source: it is only in the ray optics limit that the image of a point is a point, but the solution to the Maxwell's equations will obey the Rayleigh diffraction limit.

If we now consider the case of the Pendry-Veselago slab lens, for any pair of object points $\mathbf{x}_O$ and $\mathbf{x}_{O'}$, their images fulfil $| \mathbf{x}_I - \mathbf{x}_{I'} | = | \mathbf{x}_O - \mathbf{x}_{O'} |$.

One can actually prove the impossibility of sharply imaging two object planes with non-unit magnification holds regardless of distortion requirements [40]. An image magnification m means that $| \mathbf{x}_I - \mathbf{x}_{I'} | = m | \mathbf{x}_O - \mathbf{x}_{O'} |$ and an example is provided by the homeopathy effect for the perfect cylindrical lens [5]. An interesting question to ask is whether the magnified image is perfect, and this has been actually shown by Pendry and Ramakrishna through a conformal mapping from a periodic stack of heterogeneous anisotropic perfect lenses onto the cylindrical homogeneous isotropic one [13]. Importantly, one of us actually studied the electrostatic response of a dielectric cylinder surrounded by a coating with negative permittivity back in 1994 [5]. This optical system also acts as a perfect lens, which further magnifies the image, as observed in [13].

In the same vein, it is legitimate to wonder whether all-angle-negative refraction in photonic crystals [42] refocusses a line source onto an image with a resolution lower or equal to $\lambda/3$, since evanescent waves are not amplified in this optical system. Merlin actually showed that the resolution of the Veselago-Pendry lens scales as a logarithm of the absorption within the lens [43]. Merlin further demonstrated that the absorption was linked to the spatial oscillations of surface waves at the interfaces between complementary media, and this was further numerically confirmed in general anisotropic heterogeneous complementary media of the checkerboard type [24].

The numerical simulation in the lower panel of Fig. 2 for a source radiating within the Maxwell fisheye, suggests that a perfect image is formed within the non-uniform (positive) refractive index of this most unusual lens. By comparison with the upper panel of Fig. 2, whereby the negative refractive index within the Pendry-Veselago slab lens $n = -1 + i * 0.4$, it is indeed apparent that the image displays comparable features. However, there is a major difference here: in the former case, the highly heterogeneous region surrounding the image contributes to its resolution, whereas in the latter case it is fair to say that the image is subwavelength.

10

To understand the mechanism leading to the image formation within the Maxwell fish eye, we look at the surface of the virtual sphere, within which light rays propagate along geodesics, the great circles. It is one of the remarkable properties of the stereographic projection that circles on the sphere are transformed into circles on the plane. From this we infer that in physical space, light goes around in circles as well. The great circles originating from one source point on the sphere meet again at the antipodal point. In the stereographic projection, the image of the antipodal point is the reflection of the source on a circle, the circle with the radius r_0 of the sphere.

It is then tempting to claim that the source is perfectly imaged: Maxwell's fish eye would make a perfect lens. However, this is quite an usual instrument: both the source and the image are embedded in the non-uniform refractive index profile of the fish eye. Clearly, this optical system should display some astigmatism, which is clear from the lower panel in Fig. 2: the optical system is not symmetric about the optical axis. While this is also the case of a cylindrical perfect lens [6, 23, 5], we note that astigmatism is observed even for rays from on-axis object points in the fish eye. Hence, this lens is already less than perfect. However, more importantly, the image appears in a highly heterogeneous medium (the fish eye itself) and it is therefore not simple to measure its resolution. The wavelength is obviously compressed to a tiny space, but partly because of the large refraction index.

In contrast, for the flat lens made with negative refractive index material, both source and image are outside the device and in perfect alignment about the optical axis. Note also that the lens acts across some distance, unlike confocal microscopes or other types of high-resolution optical system tomography [32].

4.2   Leonhardt's proposal of a fisheye mirror in a nutshell

The original fisheye, as first described by Maxwell, is a medium of infinite extent. We therefore needed to cut off the fisheye with some care as it focuses all rays from the object at the image, but these include rays that propagate out to arbitrarily large radius. If the fisheye is cut off carelessly, then the quality of the image might deteriorate, but this would be a mere numerical artifact. We therefore implemented PMLs within an annulus encompassing a disc which is 10 wavelengths in diameter. Transverse magnetic waves are then governed by (9) in the disc, and (12) in the annulus and numerical results are reported in Fig. 2 and Fig. 3.

However, people might argue that adding PMLs within the model still affects the numerical solution of the real open boundary problem. Moreover, the refractive index for the fisheye varies between $n = 2$ at the center and $n = 1$ on the boundary of a disc of radius $r = r_0$ (r_0 radius of the virtual sphere), and then decreases to zero at infinity. This means that the speed of light outside the disk (for $r > r_0$) is greater than c, speed of light in vacuum, and tends to infinity when r tends to infinity. A way of making a device with the same imaging capability as the infinite fisheye and avoiding such paradoxes is then to follow Leonhardt's recent proposal [33] and put a mirror at $r = r_0$. This means we now keep only (9), but importantly supply it with perfect electric boundary conditions i.e. $E_3 = 0$ in this case of polarisation. The numerical results are reported in Fig. 4 and Fig. 5.

To interpret results of Fig. 3 and Fig. 5, namely the resolution of the image within a fisheye, it is necessary to take into account the fact that the image forms in a complex medium with varying refractive index greater than that of vacuum. For this purpose, we adopt the following definition for the resolution of an image within the Maxwell fisheye:

Definition: *The resolution of the image in a heterogeneous isotropic lens is given by the ratio of the full width at half maximum of the image-point divided by the average of the wavelength λ between the source and image planes.*

If we adopt this definition, then the Maxwell fisheye has a resolution of $\lambda/3$ in TM polarisation, which is just above the Rayleigh diffraction limit. Indeed, one can see that in Fig. 3 and Fig. 5 (upper panel) that the averaged wavelength λ, is much smaller than the free space wavelength (except outside the disc of radius r_0). If one would compute the resolution with respect to free space wavelength, the image would be considered as highly subwavelength, but this is in fact just the classical effect of the wavelength contraction within any high refractive index medium (an

optical illusion!).

It is also interesting to look at the case of two line sources radiating within the fisheye mirror lens. As we can see in the lower panels of Fig. 4 and fig. 5, there are many secondary images appearing within the cavity. We also note that the resolution of the images is only about $\lambda/2$, which could attributed to the fact that the free space wavelength is twice as small as in the upper panel. It is also possible that the larger the number of sources the worse the resolution of their respective images, but this can only be conjectured at this stage.

Figure 4: *Harmonic line sources at free space wavelengths $\lambda_f = 0.2$ (a,c) and $\lambda_f = 0.1$ (b,d) radiating within a fisheye mirror of radius $r = 0.2 = r_0$ (with r_0 radius of the virtual sphere) and refractive index defined by (4): (a,c) One source at point $(0.1, 0)$; (b,d) Two sources at points $(0.1, 0)$ and $(0, 0.1)$; We note the symmetry of the modulus of the electric field $|E_3|$ about the y-axis in (a,c) and about $x = -y$ in (b,d).*

4.3 Open questions on the closed fisheye cavity

As mentioned in [33], fisheye mirrors may find some application in nanolithography, and are thus worthwhile investigating both on the academic and technological sides.

In [33], Leonhardt points out that *perfect imaging does not occur for the TM polarization where the magnetic-field vector H points orthogonal to the plane.* However, the terminology used in Leonhardt's paper refers to (10) as the TM case, whereas we refer to this polarisation as transverse electric (TE). We therefore need to study the other polarization case to backup this statement.

As mentioned earlier, this case represents a challenge in terms of modelling, because of the presence of a magnetic source. In order to provide the reader with an idea of what is going on in this case of polarisation, we decided to approximate the source by a set of two closely located line sources, with opposite charges, and this indeed result in a magnetic dipole, as can be seen
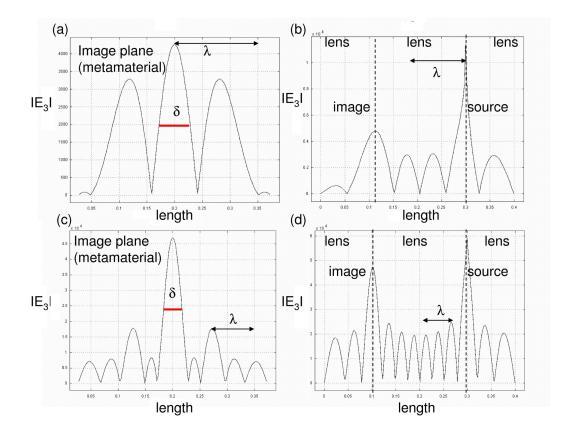
Figure 5: *Upper panel: (a) Modulus of the longitudinal electric field E_3 radiated by a harmonic line source of free space wavelength $\lambda_f = 0.2$ at point $(0.1, 0)$ in the fisheye mirror with radius $r = 0.2 = r_0$ (cf. upper-left panel of Fig. 4) along the vertical direction in the plane $x_1 = 0.12$. The red line represents the resolution of the image: full width at half maximum of the image-point is $\delta \sim \lambda/3$ (with $\lambda < \lambda_f$); (b) Profile of $\mid E_3 \mid$ in the plane $x_2 = 0$ with a source at $x_1 = 0.3$ and an image at $x_1 = 0.12$; Lower panel: (c) Modulus of the longitudinal electric field E_3 radiated by a line source of free space wavelength $\lambda_f = 0.1$ at points $(0.1, 0)$ and $(0, 0.1)$ along the vertical direction in the image plane $x_1 = -0.5$. The red line represents the resolution of the image: full width at half maximum of the image-point is $\delta \sim \lambda/2$ (with $\lambda < \lambda_f$); (d) Profile of $\mid E_3 \mid$ in the plane $x_2 = 0$ with a source at $x_1 = 0.3$ and an image at $x_1 = 0.1$.*

in Figure 6. Here, the two point sources are located a distance 0.002 apart while the free space wavelength is $\lambda = 0.1$. We set some infinite conducting boundary conditions i.e. $\partial H_3/\partial n = 0$ at $r = r_0$. We observe that the orientation of the moment of the magnetic dipole (here, along the horizontal and vertical axes) indeed matters for the reconstruction of the image, as can be seen in Fig. 7. In this case of polarisation, we have to adapt our definition of image resolution to a dipole, and it seems natural to now look at the ratio of the full width at half maximum of the dipole image points divided by the average of the wavelength λ between the source and image planes, which corresponds to the red segment in Fig. 7.

Actually, we find that the image resolution varies between $\lambda/2$ and $\lambda/4$, the latter being subwavelength. We checked that when we only consider a line source (a magnetic monopole), the resolution of the image does not exceed $\lambda/2$, and lies therefore clearly within the Rayleigh
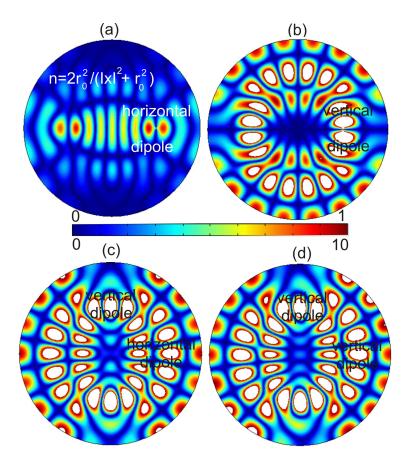
Figure 6: *Harmonic dipole sources at free space wavelength $\lambda_f = 0.1$ radiating within a fisheye mirror of radius $r = 0.2 = r_0$ (with r_0 radius of the virtual sphere) and refractive index defined by (4): (a,b) One dipole at point $(0.1, 0)$ oriented along the horizontal (a) and vertical (b) axes; (b,d) Two dipole sources at points $(0.1, 0)$ and $(0, 0.1)$ oriented along the horizontal and vertical axes; We note the symmetry of the modulus of the magnetic field $\mid H_3 \mid$ about the y-axis in (a,b,c), and the huge enhancement of the field in (c,d) requiring a color scale ten times larger.*

diffraction limit. The statement of Leonhardt is therefore fully consistent with our findings in the case of a magnetic monopole, but the answer seems less conclusive for a magnetic dipole. However, we are not yet in a position to either prove or disprove Leonhardt's statement that in the other case of polarisation (TM) *the geometry of light established by Maxwells fisheye is not restricted to rays, but extends to waves, which may explain why waves are as perfectly imaged as rays.* More precisely, according to Leohnardt, for a 2D fisheye formed by an electric permittivity with trivial magnetic permeability, only for the TM polarization (using our terminology i.e. for (9)) is wave propagation exactly equivalent to propagation on a sphere and the image of a point is a point. Our numerical results suggest that the resolution of the image still depends upon the material constituents and with our definition is about one third of the wavelength. Moreover, Leonhardt's proposal of a 3D fisheye that would image all waves perfectly refers to a medium that exactly corresponds to propagation on a hypersphere, which requires a Maxwell fisheye with equal permittivity and permeability given by Maxwell's refractive index profile.

In the course of this work, we came across other interesting features on the fisheye, apparently not discussed in the literature, which we now discuss.
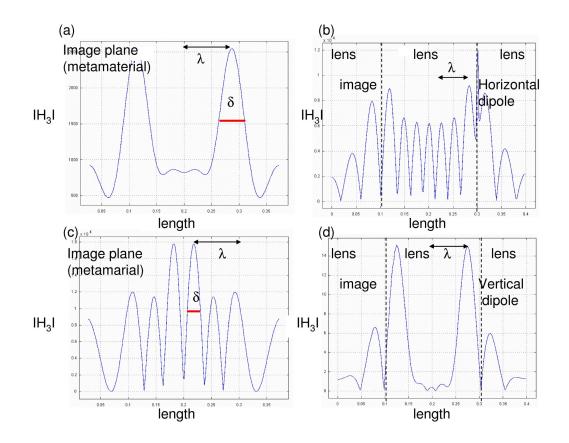
Figure 7: *Upper panel: (a) Modulus of the longitudinal magnetic field H_3 radiated by a magnetic dipole oriented along x_1 with free space wavelength $\lambda_f = 0.1$ at point $(0.1, 0)$ in the fisheye mirror with radius $r = 0.2 = r_0$ (cf. upper-left panel of Fig. 6) along the vertical direction in the plane $x_1 = 0.1$. The red line represents the resolution of the image: full width at half maximum of the image-point is $\delta \sim \lambda/4$ (with $\lambda < \lambda_f$); (b) Profile of $| H_3 |$ in the plane $x_2 = 0$ with a dipole source at $x_1 = 0.3$ and an image at $x_1 = 0.1$; Lower panel: (c) Modulus of the longitudinal magnetic field H_3 radiated by a dipole source oriented along x_2 with free space wavelength $\lambda_f = 0.1$ at point $(0.1, 0)$ in the image plane $x_1 = 0.1$. The red line represents the resolution of the image: full width at half maximum of the image-point is $\delta \sim \lambda/2$ (with $\lambda < \lambda_f$); (d) Profile of $| H_3 |$ in the plane $x_2 = 0$ with a source at $x_1 = 0.3$ and an image at $x_1 = 0.1$.*

5 Cross-over ray trajectories and multiple images in the Fisheye

There is yet another issue to address for the Maxwell fisheye: if one draws some ray trajectories emanating from two sources on the virtual sphere as in Fig. 8, it appears that there are many images resulting from the many intersection of geodesics (great circles). It looks as if the set of images is a dense subset of the surface of the sphere i.e. there are an infinite number of images. This is a very surprising feature whereby one source gives rise to one and only one image whereas two sources give rise to an infinite number of images. This ray picture is confirmed by numerical simulations in Fig. 9 which clearly show that there are more and more images when the wavelength is smaller

and smaller. When we move to higher frequencies, we observe even more images. However, when we refine the mesh solutions become less stable for higher frequencies. Our computations suggest that we would observe many more images if we could refine the mesh even further within our finite element model. The solution of the real problem lies maybe somewhere between the ray optics picture indicating an infinite number of cross-over ray trajectories on the sphere and the wave picture which suggest that the number of images depends upon the wavelength, and somewhat on the mesh used in the numerics. We believe this is a very interesting electromagnetic paradigm well worth investigating with more analytical tools to check if there are no numerical artifacts behind the wave pictures depicted here.
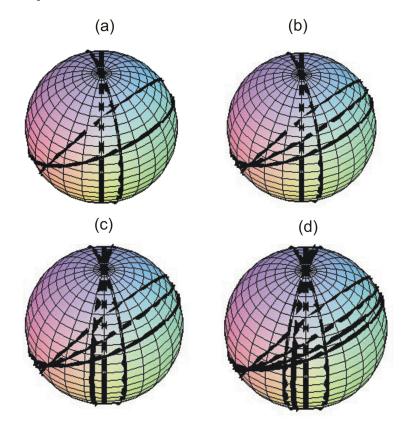

Figure 8:   *Ray trajectories for light radiating by two sources points at the surface of the virtual sphere with (a) 2 rays radiated by each source; (b) 3 rays radiated by one source and 2 rays by the other; (c) 3 rays radiated by each source; (d) 4 rays radiated by each source; Note that the more rays emanating from the two sources, the more intersections between ray trajectories and therefore the more images.*

There is an interesting analogy between the ray construction in optics and electromagnetism and the method of images in electrostatics. The former is sometimes evident in expansions like the Airy series, which treats multiple reflections between interfaces as a sum over rays. The latter can be used to form an imaging series between two dielectric interfaces when solving Laplace's equation. The interesting issue which arises then [44] is the convergence of the imaging series, which indeed is handled in electrostatics by the method of analytic continuation. The resulting expression is a function called the dilogarithm, which has a branch cut along the negative real axis of dielectric permittivity. This analogy suggests there may well be difficulties with the ray picture of electromagnetism when negative permittivities and permeabilities are present, and that field solutions embodying analytic functions embody the resolution of these difficulties.
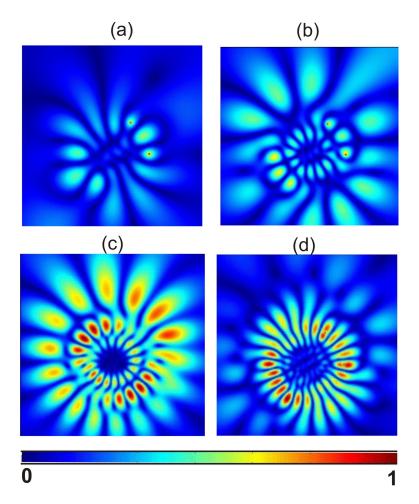
Figure 9: *Mirages effects: two sources in the Maxwell fisheye produce multiple images as shown in Fig. 8; Modulus of E_3 two harmonic line sources located at $(1.5, 0)$ and $(0, 1.5)$ radiating at free space wavelengths (a) $\lambda_f = 0.4$; (b) $\lambda_f = 0.27$; (c) $\lambda_f = 0.24$; (d) $\lambda_f = 0.2$.*

6   Coming to the point in the Eaton lens

From the previous analysis, we can see that the image resolution we obtained in the Maxwell fisheye and the silver slab lens is about one third of the wavelength in vacuum and cannot be therefore classified as deeply subwavelength. However, in the former lens, both source and image lie within a heterogeneous medium, whereas in the latter, they are located in air (and far from the interface metamaterial-air). Therefore, we are facing a dilemma as none of these lenses clearly meets the requirement for a perfect lens (i.e. the image beats the diffraction limit): they are borderline. However, in the case of the silver slab lens, we know that the resolution is limited by the absorption in the negative refractive index medium, and the image is also formed in vacuum, and far from the interface between metamaterial and air (confocal microscopes can indeed reach a resolution of $\lambda/20$, however only in the intense near field limit). From the 2005 experiment of Zhang's team, a resolution of $\lambda/6$ has only been achieved with a thin film of silver, and alternating layers of silver and dielectric might further improve this resolution [13].

We thus proceed with a last example of conjugate optical imaging system, known as the Eaton

lens [45]. In that case, the refractive index is defined as follows:

$$n = \begin{cases} 1 & , \quad \text{for } \sqrt{x^2 + y^2} < 1 , \\ \sqrt{\frac{2}{\sqrt{x^2+y^2}} - 1} & , \quad \text{for } 1 \le \sqrt{x^2 + y^2} < 2 . \end{cases}$$

The refractive index is not defined outside the disc $\sqrt{x^2 + y^2} \le 2$. On the boundary of this disc, perfect conducting boundary conditions are imposed i.e. the lens is surrounded by a mirror.
We note that the refractive index in the ring $1 \le \sqrt{x^2 + y^2} < 2$ is lower than that of the unit disc which is filled with air. This explains why the averaged wavelength λ between the source and image planes appears to be smaller than the wavelength in the image plane (filled with $n < 1$) in Fig. 11.
Ray trajectories inside the unit disc are obviously straight lines ($n = 1$) and since the refractive index is always symmetric about $x = 0$, it is easily seen that any source has a mirror image such that $\mathbf{x}_I = -\mathbf{x}_0$.
This prediction of the ray optics limit corresponds to what we obtain with the full wave solution, see Fig. 10. However, the image resolution we computed from Figs. 10 and 11 is about half of the averaged wavelength. It seems therefore fair to say that while the geodesics in the Maxwell fisheye and the Eaton lens suggest focusing of a source comes to an image point, this theoretical prediction breaks down when look for subwavelength imaging by solving the Maxwell equations. Negative refraction makes a perfect lens, but the Maxwell fisheye allows for conjugate images in the ray optics limit.
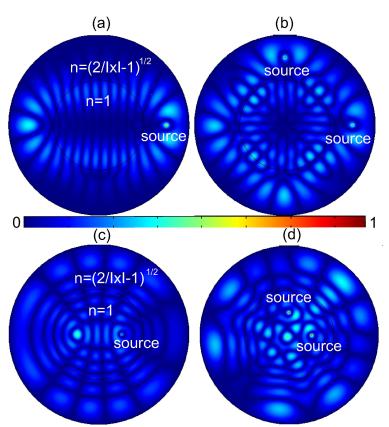

Figure 10:   *Harmonic line sources at wavelength $\lambda = 0.4$ radiating within an Eaton lens of radius 0.2 and refractive index defined by (16): (a) One source at point $(1.5, 0)$; (b) Two sources at points $(1.5, 0)$ and $(0, 1.5)$; (c) One source at point $(0.5, 0)$; (d) Two sources at points $(0.5, 0)$ and $(0, 0.5)$.*
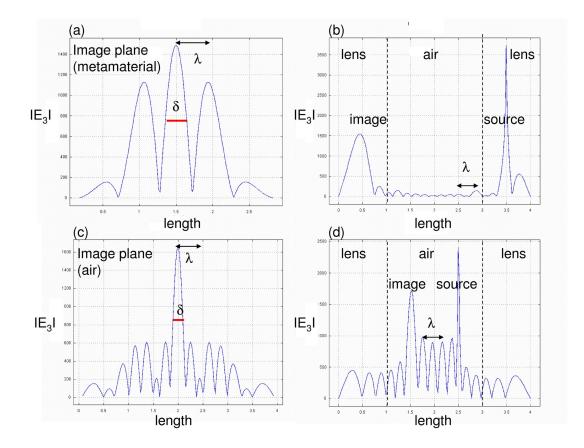
18

Figure 11: *Upper panel: (a) Modulus of the longitudinal electric field E_3 radiated by a line source of free space wavelength $\lambda_f = 0.2$ at point $(1.5, 0)$ in the Eaton lens (cf. upper-left panel of Fig. 10) along the vertical direction in the plane $x_1 = -1.5$. The red line represents the resolution of the image: full width at half maximum of the image-point; (b) Profile of $\mid E_3 \mid$ in the plane $x_2 = 0$; Lower panel: (c) Modulus of the longitudinal electric field E_3 radiated by a line source of free space wavelength $\lambda_f = 0.1$ at point $(0.5, 0)$ (in air) in the Eaton lens (cf. lower-left panel of Fig. 10) along the vertical direction in the image plane $x_1 = -0.5$. The red line represents the resolution of the image: full width at half maximum of the image-point; (d) Profile of $\mid E_3 \mid$ in the plane $x_2 = 0$.*

7 Concluding remarks

In conclusion, we have presented a comprehensive variational analysis of the Fermat's principle leading to the equation for geodesics. We further investigated the design of the Maxwell fisheye and the Pendry-Veselago slab lens using transformation optics. This enabled us to notice three main differences between these optical systems: the former displays some astigmatism while the latter does not; the former focusses a source onto an image in a heterogeneous medium while the latter displays an image in vacuum; the former shows an infinity of secondary images in the case of two sources while the latter only shows two images. We numerically noted that the Maxwell fisheye and a silver slab lens both display a resolution of $\lambda/3$ in the transverse magnetic case (electric field pointing orthogonal to the plane), which can be considered borderline for super-resolution. In the transverse electric polarisation, the resolution of the image (a dipole) varies between $\lambda/2$ and $\lambda/4$ depending upon the orientation of the magnetic moment of the dipole source. However, when

19

we looked at the Eaton lens, the fact that its resolution does not exceed $\lambda/2$ confirms us in our opinion that while a negative refractive index can lead to subwavelength imaging, the limit of image resolution (and its very definition) within a Maxwell fisheye is far from being obvious.

Forbes and Wallace have noted back in 1995, that there is a fine line between the system performance displayed by a lens in geometrical optics and the resolution which can effectively be attained from full wave computations [46]. However, Leonhardt has mathematically shown [33] that for a Maxwell fisheye with a mirror at $r = r_0$ that the analytical form of the Green's function provides the right logarithmic singularity to expect a perfect image in the transverse magnetic case (electric field pointing orthogonal to the plane), unlike for the transverse electric case. Our numerical results are thus less contrasted. Leonhardt further claims in [33] that a three-dimensional version of the Maxwell fisheye (i.e. constructed from a 4D hypersphere) would make a perfect lens without negative refraction. While this proposal seems to be a promising route towards the design of new transformation based optical devices, the numerical study required to prove the subwavelength features of this less than ordinary lens lies beyond the scope of the present paper.

In our opinion, while the Maxwell fisheye is in itself a fascinating optical system, it rather forms conjugate images than perfect images, at least in two dimensions [33]. We agree that all rays emanating from a source converge to an image, thereby forming a sharp image in the ray optics limit. However, negative refraction is a prerequisite for existence of plasmons enabling the amplification of the evanescent component of the near field radiated by the source, thereby clearly making the image subwavelength in the absence of strong absorption or losses. While it might be too much to ask a thick slab of silver to act as a perfect lens for some optical wavelength, an alternation of thin silver films and dielectrics as first proposed in [15] might work just fine. It is also possible to surround the slab of silver with air on one side and other media such as glass or GaAs on the other to make an asymmetric lossy near-perfect lens an alternation of thin silver films and dielectrics as first proposed in might work just fine [13].

The renewed interest in classical lenses such as the Maxwell fisheye is fueled by the original viewpoint of transformation optics, which is a burgeoning field still in its infancy. Analogies with general relativity whereby the interplay of gravitational waves with space-time metric becomes more apparent when equations are written in covariant forms lead to fascinating devices based on projections from upper-dimensional spaces. For instance, the design of a 3D non-singular cloak or a 3D Maxwell fisheye requires analysis of geodesics on a hypersphere [47]. These represent unprecedent challenges for computational electromagnetism associated with physical paradigms of interest for a general audience. Correspondences with other areas of physics where governing equations are transformation invariant such as quantum physics, elastodynamics, fluid dynamics have already been noticed [48, 49, 50, 52, 51]. Needless to say that new discoveries are on their way and anyone wishing to take part in this cutting-edge research might become pioneer of a new field of science in his/her own right.

Acknowledgements

References

[1] V.G. Veselago 1967, Usp. Fiz. Nauk **92**, 517.

[2] J.B. Pendry, A.J. Holden, D.J. Robbins and W.J. Stewart 1996, Phys. Rev. Lett. **76**, 4763.

[3] J.B. Pendry, A.J. Holden, W.J. Stewart and I. Youngs 1999, IEEE Trans. Micr. Theo. Tech. **47**, 2075-2084.

[4] N.A. Nicorovici, R.C. McPhedran, G.W. Milton 1994, Phys. Rev. B **49**, 8479-8482.

[5] G.W. Milton, N.A. Nicorovici, R.C. McPhedran and V.A. Podolskiy 2005, Proc. R. Soc. Lond. A **461**, 3999-4034.

[6] G.W. Milton and N.A. Nicorovici 2006, Proc. R. Soc. Lond. A **462**, 3027-3059.

[7] G.W. Milton, N.A. Nicorovici, R.C. McPhedran, K. Cherednichenko and Z. Jacob 2008, New J. Phys **10**, 115021.

[8] D.R. Smith, W.J. Padilla, V.C. Vier, S.C. Nemat-Nasser and S. Schultz 2000 Phys. Rev. Lett. **84**, 4184.

[9] J.B. Pendry 2004 Contemp. Phys. **45**, 191.

[10] S.A. Ramakrishna 2005 Rep. Prog. Phys. **68**, 449.

[11] G.W. Milton 2002 *The Theory of Composites* (Cambridge: Cambridge University Press)

[12] J.B. Pendry 2000 Phys. Rev. Lett. **85**, 3966.

[13] S. Anantha Ramakrishna, J.B. Pendry, D.R. Smith, D. Schurig and S. Schultz 2002, J. Mod. Optics **49**, 1747-1762.

[14] D.R. Smith, D. Schurig, M. Rosenbluth, S. Schultz, S. Anantha Ramakrishna and J.B. Pendry 2003, Appl. Phys. Lett. **82**, 1506.

[15] S.A. Ramakrishna, J.B. Pendry, M.C.K. Wiltshire and W.J. Stewart 2003, J. Mod. Optics **50**, 1419-1430.

[16] J.B. Pendry, D. Schurig and D.R. Smith 2006, Science **312**, 1780.

[17] D. Schurig, J.J. Mock, B.J. Justice, S.A. Cummer, J.B. Pendry, A.F. Starr and D.R. Smith 2006, Science **314**, 977-980.

[18] U. Leonhardt 2006, Science **312** 1777.

[19] U. Leonhardt 2006, New. J. Phys. **8**, 118.

[20] A. Greenleaf, M. Lassas and G. Uhlmann 2003, Math. Res. Lett. **10**, 685-693.

[21] U. Leonhardt and T.G. Philbin 2006, New J. Phys. **8**, 247.

[22] S. Guenneau and S.A. Ramakrishna, Comptes rendus - Physique, DOI: 10.1016/j.crhy.2009.04.002

[23] J.B. Pendry and S.A. Ramakrishna 2003, J. Phys. Cond. Matter **15**, 6345.

[24] S. Guenneau, B. Gralak and J.B. Pendry 2005, Opt. Lett. **30**, 146.

[25] M. Notomi 2002, Opt. and Quant. Elec. **34**, 133.

[26] S. He, Y. Jin, Z. Ruan and J. Kuang 2005, New J. Phys. **7**, 210.

[27] S. Guenneau, A.C. Vutha and S.A. Ramakrishna 2005, New J. Phys. **7**, 164.

[28] S. Chakrabarti, S.A. Ramakrishna and S. Guenneau 2006, Opt. Express **14** 12950-12955.

[29] U. Leonhardt and T. Tyc 2009, Science **323**, 110

[30] T. Tyc and U. Leonhardt 2008, New J. Phys. **10**, 115038.

[31] U. Leonhardt and T. Tyc 2008, New J. Phys. **10**, 115026.

[32] G. Maire, F. Drsek, J. Girard, H. Giovannini, A. Talneau, D. Konan, K. Belkebir, P. C. Chaumet and A. Sentenac 2009, Phys. Rev. Lett. **102**, 213905.

[33] U. Leonhardt 2009, New J. Phys. **11**, 093040

[34] B. Dacorogna, Introduction to the calculus of variations (Imperial College Press, 2004).

[35] U. Leonhardt and T.G. Philbin 2009, Prog. Opt. 53, 70-152.

[36] N. Fang, H. Lee, C. Sun and X. Zhang 2005, Science **308**, 534.

[37] J.P. Berenger 1994, Journal of Computational Physics **114**, 185-200.

[38] M. Lassas and E. Somersalo 2001, Proceedings of the Royal Society of Edinburgh, Sect. A. Mathematics **131**, 1183-1207.

[39] A. Nicolet, F. Zolla, Y. Ould Agha and S. Guenneau 2008, International Journal for Computation and Mathematics in Electrical and Electronic Engineering COMPEL **27**, 806-819.

[40] M. Born, E. Wolf, Principles of Optics, (Pergamon, Oxford, 1989).

[41] J.C. Minano 2006, Opt. Express **14**, 9627-9635.

[42] B. Gralak, S. Enoch and G. Tayeb 2000, J. Opt. Soc. Am. A **17**, 1012-1020.

[43] R. Merlin 2004, Appl. Phys. Lett. **84**, 1290.

[44] R.C. McPhedran and G.W. Milton 1987, Proc. Roy. Soc. A **411**, 313-326.

[45] R.K. Luneburg, Mathematical Theory of Optics, (University of California Press, Los Angeles 1964).

[46] G.W. Forbes and J.K. Wallace 1995, J. Opt. Soc. Am. A **12**, 2064-2071.

[47] U. Leonhardt and T.G. Philbin, Perfect imaging with positive refraction in three dimensions (arXiv:0911.0552v1)

[48] Milton, GW; Briane, M; Willis, JR, New J. Phys. **8** 248 (2006).

[49] M. Farhat, S. Enoch, S. Guenneau et A.B. Movchan, Broadband Cylindrical Acoustic Cloak for Linear Surface Waves in a Fluid, Physical Review Letters 101, 134501, 2008

[50] S. Zhang, D.A. Genov, C. Sun and X. Zhang, Phys. Rev. Lett. **100**, 123002 (2008).

[51] M. Farhat, S. Enoch, S. Guenneau and A.B. Movchan, Phys. Rev. B **79** 033102 (2009).

[52] M. Brun, S. Guenneau and A.B. Movchan, Appl. Phys. Lett. **94** 061903 (2009).